Cross-structures Deep Transfer Learning through Kantorovich potentials for Lamb Waves based Structural Health Monitoring

Hadrien Postorino, Eric Monteiro, Marc Rebillat, Nazih Mechbal

Cross-structures Deep Transfer Learning through Kantorovich potentials for Lamb Waves based Structural Health Monitoring

Hadrien Postorino *[1], Eric Monteiro †[1], Marc Rébillat ‡[1], and Nazih Mechbal §[1]

[1] *Arts et Métiers Institute of Technology, CNAM, PIMM, HESAM University, 151 boulevard de l'Hopital, 75013, Paris, France*

Abstract

In Lamb Waves based Structural Health Monitoring (LWSHM) of composite aeronautic structures, Deep Learning (DL) methods have proven to be promising to monitor damage using the signals collected by piezoelectric sensors (PZTs). However, those data driven algorithms are strongly problem dependent: any structural change dramatically impacts the accuracy of the predictions and the generalization of the learnt algorithms to other structures within the fleet is impossible. Transfer Learning (TL) promises to face that issue by capitalizing on the knowledge acquired on a given structure to transfer it on another from the fleet. An original TL approach based on the Optimal Transport (OT) theory is proposed here to handle this issue. OT provides a rigorous mathematical framework for TL that can be practically implemented using Input Convex Neural Networks modelling Kantorovich potentials but that has never been used for LWSHM. Using OT, the knowledge acquired on a rich LW database is transferred to poorer LW databases collected on different structures with rising structural divergences. A Structural Index (SI) is defined and used to compute the gap between those different structures and can be used to estimate a priori the necessity of the use of TL methods. The proposed OT based TL method for LWSHM manages to reduce by almost 50% the predictions errors between numerical structures with strong differences (bias in mechanical properties and erroneous PZT position) in comparison with standard approaches. That leads to a promising approach to

Journal of Structural Dynamics

combine rich numerical database with poorer database in order to build robust algorithms for LWSHM of a fleet of aeronautical composite structures.

Keywords: Data-driven Lamb Waves SHM; CNN; Monge-Kantorovich duality; Deep Transfer Learning; Fleet monitoring

Acronym	Definition
LW	Lamb Waves
SHM	Structural Health Monitoring
NDE	Non Destructive Evaluation
PZT	Piezoelectric element
DI	Damage Index
SI	Structural Index
DL	Deep Learning
TL	Transfer Learning
OT	Optimal Transport
CNN	Convolutional Neural Network
ICNN	Input Convex Neural Network
DA	Domain Adaptation
JDA	Joint Domain Adaptation
JDOT	Joint Distribution Optimal Transport
TCA	Transfer Component Analysis
ARTL	Adaptive Regularization based Transfer Learning
MMD	Maximum Mean Discrepancy
MSE	Mean Square Error

Table 1: Table of acronyms

1 Introduction

1.1 Lamb Waves based Structural Health Monitoring (LWSHM)

Structural Health Monitoring (SHM) is a powerful tool for the deployment of condition-based maintenance in many industrial sectors [1]. SHM promises to reach cost and weight reductions, design optimizations, and increased durability. SHM and Non Destructive Evaluation (NDE) share the same objective which is to ensure that the structure under study is not damaged but with one major difference. In the case of NDE, there is a

*hadrien.postorino@ensam.eu
†eric.monteiro@ensam.eu
‡marc.rebillat@ensam.eu
§nazih.mechbal@ensam.eu

human operator handling a NDE instrument who is carrying the interrogation procedure and who is deciding whether the structure is damaged or not. In SHM, the actuators and sensors are permanently installed within the host structure and algorithms are deciding whether the structure is damaged or not. SHM can thus be seen as an automated version of NDE relying on permanently installed transducers. New kind of structures, called *smart structures* are thus equipped with sensors and actuators to give them new functionalities. We focus here on the health monitoring of a fleet of smart composite structures based on Lamb Waves (LW) generated and measured by a network of piezoelectric patches (PZT)s implemented on the structures. The reversibility of the piezoelectric effect allows using the patches alternatively as sensors or actuators. LWs propagate at high velocity with low attenuation in thin layers [2–4], thus an inspection of large parts can be achieved with a relatively low number of PZTs and very rapidly. However, LWs propagation in the host structure is hard to analyze: several symmetric and antisymmetric modes can propagate simultaneously in the composite structures at the same frequency, LWs interact with the interfaces, they reflect on the borders, etc. LW based SHM thus relies on advanced signal processing tools, physics-based models, as well as data-driven models to extract information about a potential damage from the measured data [5, 6]. The information to be gathered for damage monitoring should handle the four levels of SHM proposed by Rytter regarding damage knowledge [7] : (i) Detection, (ii) Localization, (iii) Classification and (iv) Quantification.

Damage detection using Lamb waves is a task that can be easily performed and there exists numerous algorithms able to do so [8, 9]. Damage localization is more delicate to achieve, and even if Lamb waves based algorithms exist, there is still room for improvement in that area [10–12]. Damage classification, is harder to achieve and to test in practice as several damage types are needed, which is complicated to manage in practice for composite materials [9, 13]. Finally, the damage quantification step is the most delicate one and is a current area of research [14, 15]. Consequently, the focus is here put on the damage localization and severity quantification steps of the LWSHM process.

1.2 Deep learning based LWSHM intrinsic limitations

Deep Learning (DL) great successes in image processing [16] or sound analysis [17] encourage its use to achieve the four SHM tasks mentioned previously. The damage detection based on DL has been successfully proposed by many papers [18–26]. Damage classification is more difficult because of the large diversity of damages that can be encountered in practice in composite structures, however anomaly classification was achieved successfully in [19, 24–28]. The damage localization step is achieved easily

when one kind of damage is generated in the dataset [18, 22, 23, 29, 30]. Damage quantification strongly depends of the damage classification step, but if the damage type is known, DL methods estimate properly its size [21, 28, 30, 31].

Most of the previous papers trains their models with experimental data obtained on simple case studies such as plates [20, 21, 26, 27, 30–32], gearboxes [24, 25], or storey structures [18, 28, 33]. Those approaches are trained on large dataset impossible to acquire practically in an industrial context because of their cost and the lack of information on the damage. Numerical dataset are easier to generate [19, 23, 29] but there is still an existing gap between the numerical models and the experimental reality that prevents their use in practice as the simuated numerical models do not exactly correspond to the actual reality. As input data format, some papers use the temporal signals directly [20, 30], others transform the data in 2D images (for example using time-frequency transforms) [26, 34], and others compute specific SHM features such as Damage Indexes (DIs) [21], Time Varying Damage Indexes [32] or localization figures [31]. The architecture of the DL networks strongly influence the accuracy of the model. It must be adapted to the data format and the dataset size. Most of the papers uses Convolutional Neural Networks (CNNs) [18–27, 29–31] but other types of architecture present good results in [29] or [18] .

This brief overview shows that despite the difficulties inherent to data acquisition in LWSHM, CNN and others DL architectures obtain interesting results and deserve to be deployed to solve the SHM tasks. These data-driven methods however inevitably depends on training data that are difficult and costly to collect: in SHM there is rarely enough experimental data to train a DL model. The learning obtained also depends on the structure that produced the data: any structural, geometrical, sensor or environmental variation modifies the propagation of the waves and risks to degrade the predictions accuracy. Training the models with numerical data is thus mandatory because of the experimental cost, but the gap between the numerical models and the reality strongly degrades the performances of the trained DL models and their use is impossible in many cases. Furthermore, two similar aeronautic structures to be monitored (as would be expected for fleet monitoring) are not identical: there exists variability on piezoelectric elements positions and material properties or differences in service history, just to name a few. A DL algorithm trained on such a structure may thus not be generalized directly to another structure if it is too different and must be retrained or adapted to the new target structure. These various drawbacks thus strongly impact the practical usefulness of DL approaches for LWSHM despite promising initial results.

1.3 Transfer Learning

Transfer Learning (TL) seeks to capitalize on the knowledge acquired in solving a problem to apply it to another relatively close problem [35, 36], and appears to be a solution to the issues mentioned before. TL relies on the concepts of domain and task. A **domain** $\mathcal{D}$ consists of a feature space $\mathcal{X}$ associated with the marginal probability distribution $\mu(X)$, a finite sample of features data $X = x_1, ..x_n \in \mathcal{X}$ and the labels $\mathbf{y} \in \mathcal{Y}$. A **task** $\mathcal{T}$ associates a label space $\mathcal{Y}$ with a decision function $f : \mathcal{X} \rightarrow \mathcal{Y}$ such that $\mathcal{T} = \{\mathcal{Y}, f(\cdot)\}$. It aims to associate to a new data $x \in \mathcal{X}$ a label $y \in \mathcal{Y}$ using the function f. In supervised learning, this task is learned from a set of data and label pairs x_i, y_i with $x_i \in X$ and $y_i \in \mathcal{Y}$.

The **source domain** is denoted $\mathcal{D}^s = \{\mathcal{X}_s, \mu_s(X)\}$ with n_s labels $\mathcal{Y}_s$ and the source task $\mathcal{T}_s = \{\mathcal{Y}, f_s\}$. On this domain, the amount of data is sufficient to learn easily the task $\mathcal{T}_s$. The **target domain** $\mathcal{D}^t = \{\mathcal{X}_t, \mu_t(X)\}$ with the n_t labels $\mathcal{Y}_t$ and the task $\mathcal{T}_t = \{\mathcal{Y}_t, f_t\}$ is defined in a similar way. The TL aims to improve the performance of the function $f_t(.)$ to learn the task $\mathcal{T}_t$ by discovering and transferring the latent knowledge from $\mathcal{D}_s$ to $\mathcal{D}_t$, where $\mathcal{D}_s \neq \mathcal{D}_t$ and/or $\mathcal{T}_s \neq \mathcal{T}_t$. Moreover, in most cases, the size of $\mathcal{D}_s$ is much larger than that of $\mathcal{D}_t$, i.e. $n_s \gg n_t$.

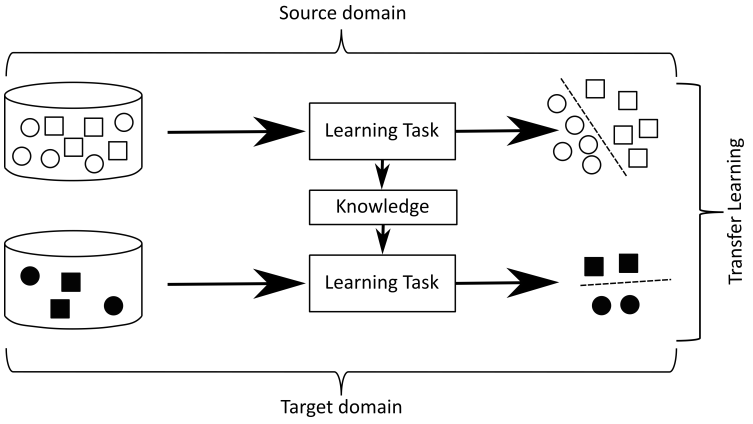

Fig. 1: Simple illustration of TL: the source task seeks to distinguish hollow squares from hollow circles. The target task seeks to distinguish solid circles from solid squares with the help of the knowledge acquired on the source task.

The approaches combining DL strategies with TL can be grouped in 4 categories [37] briefly discussed in the following.

1.3.1 Instances-based

Instances-based TL selects some instances from the source domain as supplements to the training set in the target domain. A distance computes the gap between the instances

of both domains. Only close samples are preserved via a weighting strategy to impose similar distributions between the two domains.

1.3.2 Mapping-based

Mapping-based TL maps the data from the source and the target domain into a new common space of representation. A probabilistic error is generally used during the training of the DL models to find features with aligned distributions between both target and source domains. The Joint Distribution Adaptation (JDA) proposed by [38] seeks to simultaneously align the marginal and conditional distributions of the source and target domains with a penalization strategy based on the Maximum Mean Discrepancy (MMD). The JDA is used to transfer the knowledge between two gearboxes monitored by accelerometers [39], to quantify damage in different structures in [40]. In the Joint Distribution Optimal Transport (JDOT) [41], a distance coming from the optimal transport theory is used to constrain a CNN to compute common features in both domains. Outside the framework of DL, many TL methods based on Domain Adaptation (DA) map manual features into a new space of representation. An exemple, the Population Based SHM defined in [33] maps features between a population of storey structures. Following the same concepts, DA methods compensate the effects of repairs in a composite aircraft wing in [42]. The Transfer Component Analysis (TCA) introduced in [43] is used in [44] to calibrate a digital twin of a drilling process without any prior label on the target domain. In [45], the TCA bridges the gap between the numerical model and the real storey structure to estimate a damage location with bayesian model updating.

1.3.3 Network-based

Network-based TL re-uses a fully trained model on the source domain to partially re-train it on the target domain data. During the re-training (or *fine tuning*), only a part of the weights is modified (generally the weights of the deepest layers) and the learning rate is deliberately kept low to slightly modify the model without forgetting the knowledge learned in the first phase. This approach is applied in [46] to compensate some variations in sensor positions in the monitoring of a dam. In [47], a CNN is partially re-trained by minimizing the MMD between the features extracted in rail monitoring. A CNN trained for image classification is retrained to detect damages with a camera filming a dam in [48].

1.3.4 Adversarial-based

Two adversarial models are trained simultaneously to find common representations between the source and target domains [49, 50]. A first model solves the tasks by giving labels to the data. A second model analyses the features extracted on an intermediate layer to determine whether the data is coming from the source or target domain. By penalizing the first model by the performance of the second, it becomes possible to constrain the computation of common representations for both domains.

1.4 Achieving efficient TL for LWSHM

In LWSHM, the source domain comes from an initial structure under known operating conditions or from a numerical model and the target domain comes from a structure with different properties (geometry, sensor positions, operating conditions, mechanical properties, etc.). Two similar structures to monitor, or a real structure and its numerical counterpart, can be considered as relatively close problems. The TL methods can be useful to compensate the structural and environmental variability that reduces the model's accuracy and facilitate the generalization ability of DL models. They give the possibility to use the knowledge acquired on a rich numerical dataset to transfer it to an experimental dataset with fewer labelled data. They also give the possibility to reduce the size of the training dataset and thus the cost of new DL models for SHM.

1.4.1 Mapping-based TL approaches in SHM and existing limitations

Mapping-based TL has already shown interesting results in LWSHM, especially to follow a population of similar coupons [28, 33, 51]. The tools currently developed to address this issue are looking for a new mathematical space in which the marginal probabilites, the conditional probabilities, or both of these distributions are similar and thus where it is possible to perform the desired adaptation task. In the context of SHM, three methods have been explored for this purpose. Transfer Component Analysis (TCA) proposes to learn a nonlinear transformation of the initial space that makes the marginal probabilities close in this new space. Joint Domain Adaptation (JDA) seeks to learn a nonlinear transformation of the initial space that approximates the marginal probabilities and the conditional probabilities. Rather than first searching for a new space and then learning the task in this new space, the Adaptive Regularization based Transfer Learning (ARTL) method proposes to couple the two actions within the same optimization. Those methodologies are potentially relying on known predictions and the choice of the nonlinear transformation to apply to move to the desired space remains empirical. They furthermore rely on large amounts of data to achieve their learning phases.

1.4.2 Optimal Transport advantages to achieve TL for LWSHM

The theory of optimal transport looks for the most economical solution to move objects from a set of starting points to a set of destination points [52]. The idea behind optimal transport is therefore to seek the best transformation to perform this operation through a function evaluating the cost of this transport. This idea is close to domain adaptation in the sense that is exactly a question of defining how to transform the marginal distribution associated to the target space so that it is similar to the marginal distribution associated to the source space through a dedicated cost function. Recent mathematical developments associated with this theory have proven that: i) the existence of a minimum of the cost function associated with the optimal transport is guaranteed, ii) this minimum can be found in the form of a convex function, iii) this convex function is accessible in practice, and iv) Input Convex Neural Networks (ICNN) can learn this convex function for optimal transport.

Thus, the solution of the optimal transport problem can be achieved by machine learning and is based on sound mathematical foundations that guarantee the minimization of a relevant cost function. The use of optimal transport theory in machine learning is relatively recent and has not yet been applied to SHM. Compared to the TCA, JDA and ARTL methods, the optimal transport based methods do not make any assumption about the underlying nonlinear transformation to be applied but discovers it via learning an ICNN network. This potentially leads to better generalization properties and potentially relies on much less data than traditional mapping based TL approaches.

Furthermore, as the proposed strategy relies on an ICNN, it integrates naturally within any ML frameworks or algorithms. However, the approach proposed here can be applied on any set of features, being extracted using machine learning algorithms, or more classically being empirically manufactured. Indeed, the proposed OT TL approach can transport any features set and do not necessary rely on a ML algorithm. However, as it has been emphasized previously, the implementation proposed here rely on ICNN and thus can be very naturally integrated with in a ML framework. Finally, in [9] the classification performances using empirically defined features or raw LW signals have been compared. The results have shown that using the raw LW signals leads to the best performances. This explains why it has been chosen here to illustrate the proposed approach on the basis of an initial CNN algorithm fed by raw LWs signals.

1.4.3 Contributions

As a first contribution of this work, we define an index called Structural Index (SI) allowing to evaluate quantitatively the proximity between different similar structures

equiped with PZT elements and to be monitored using LWs. The SI computed with healthy measurements on structures is a relevant index to determine the proximity between two structures and can be used to estimate *a priori* the necessity of the use of Transfer Learning (TL) methods.

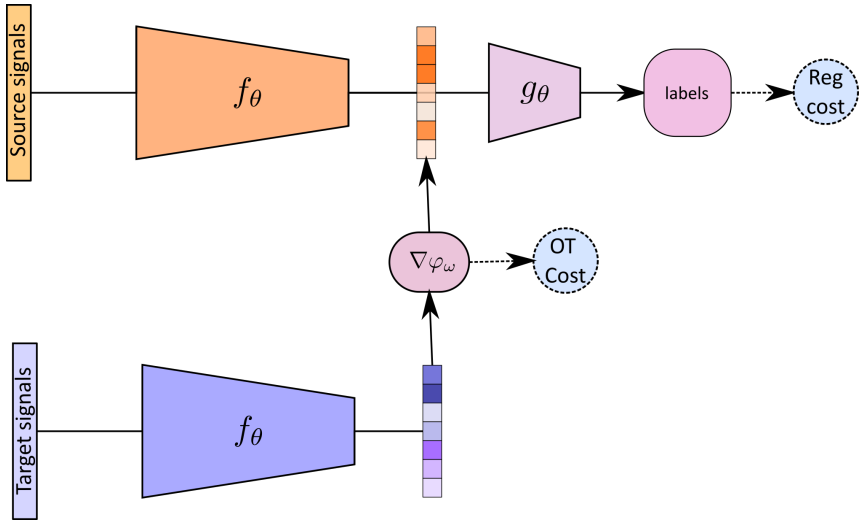

Fig. 2: Illustration of Deep Transfer Learning through Kantorovich potentials for the transportation of LWSHM features. An initial CNN built up with a feature extractor f and a classifier g is first learnt on source signals. Then, the Kantorovich potential $\nabla\phi$ implemented using ICNN and allowing to perform optimal transport is learnt on the basis of very few target signals. Using the initial CNN (i.e. the previously learnt f and g) and the Kantorovich potential (i.e. $\nabla\phi$, learnt on very few signals), it is thus possible to perform classification on the target domain on the basis of f and g learnt on the source domain.

The second contribution of the manuscript is to make a proof of concept of the application of OT and ICNN to LWSHM. Our approach aims to transport the LWSHM features computed at a deep layer of a CNN from the target domain to the source domain by applying the Optimal Transport (OT) theory to correct the misalignment between the two domains. This approach belongs to two categories mentioned above: it is both *Mapping-based* and *Adversarial-based*. Similarly with the JDOT [41] method, the OT cost quantifies the gap between the features distributions in the target and source domains and constrains the CNN to learn common features. Moreover, in our approach, the transport cost is computed using neural networks trained in parallel, leading to an adversarial-based approach.

An initial CNN is designed to estimate the position and severity of a damage on the source dataset. It is duplicated into two networks (Figure 2): the first one called **source model** $\mathcal{M}_\theta^s$ is a simple composition of the convolutional part f_θ and the fully connected part g_θ. The **target model** shares the same convolutional and fully connected parts with the source model, but at the L-th layer, another model φ_ω is inserted to apply the

optimal transport. Thus, we have by a simple composition of the relations:

$$\begin{aligned} \mathcal{M}_{\theta}^{s} &= g_{\theta} \circ f_{\theta} \\ \mathcal{M}_{\theta,\omega}^{t} &= g_{\theta} \circ \nabla\varphi_{\omega} \circ f_{\theta} \end{aligned} \tag{1}$$

with $\mathcal{M}_{\theta}^{s}$ the source model, $\mathcal{M}_{\theta,\omega}^{t}$ the target model, f_{θ} the features extraction part, g_{θ} the discriminative part, $\nabla\varphi_{\omega}$ the gradient of the Kantorovich potential which corresponds to the transport operator. We choose here to use a supervised approach: we use labels in the target domain. The proposed approach can simply be adapted in the case of an unsupervised or semi-supervised transfer with some assumptions on the distributions of the labels of both domains. One of the advantages of our approach is that the transport is not only penalizing the discrepancy between the features of the two domains but also correcting this discrepancy by applying the transportation.

1.4.4 Organization of the paper

The Section 2 defines the different numerical case study that will be tested and highlights the need of TL in SHM. The Section 3 briefly summarizes the results of OT theory that are necessary within the manuscript. The Section 4 describes the algorithms used in the proposed approach. The results of the method are presented in the Section 5 to transfer knowledge between relatively close structures. Finally a discussion on the results and the future works are proposed in Section 6.

2 Candidate datasets for Transfer Learning

2.1 Finite-element modelling of composite structures

We use the software SDTools [53] to run the simulations corresponding to the numerical cases that will be used here to assess transfer learning. The structures are modeled with shell elements with a linear elastic orthotropic behavior and meshed by a regular grid of 1mm length. The damping introduced in the model is proportional to the stiffness matrix with a coefficient $\beta = 1.5e-8$ and free mechanical boundary conditions are chosen. The model of the healthy state of the first structure has been fitted with Lamb waves measures on an equivalent experimental structure to ensure the production of realistic data (Figure 3). More precisely, this means that experimental measurements on rectangular panels made of the same composite material and equiped with PZTs have been performed. A finite-element model corresponding to that case study have then been built and updated in order to ensure a correct agreement between

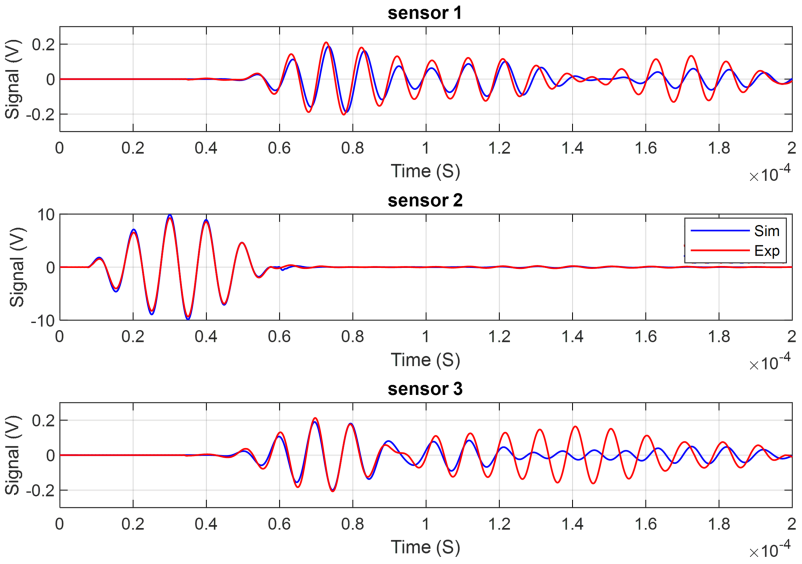

Fig. 3: Fitting of the numerical structure with its equivalent experimental structure with the PZT 2 as actuator at healthy state

the numerical predictions and the experimental measurements. These precautions have been taken in order to ensure that the numerical models used here provide numerical results representative of actual measurements. On Figure 3 it can be seen that a good correspondance between the numerical and experimental signals is indeed achieved.

2.2 Candidate Numerical Cases

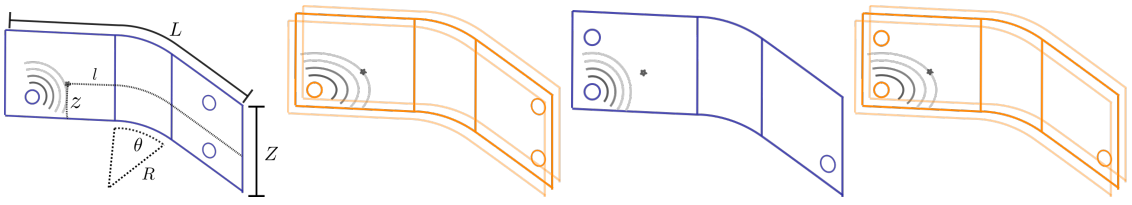

(a) C_0 : Source **(b)** C_1 : Bias and uncertainties **(c)** C_2 :Bad PZT position **(d)** C_3 : Bias, uncertainties and erroneous PZT position

Fig. 4: Studied structures

We consider four curved composite smart structures represented by their finite element models (see Figure 4 and Table 2). For the four models, the damage is modeled by a reduction of stiffness on cylinder crossing the structure thickness with a diameter of 10 mm. What is called "severity" here corresponds to a stiffness reduction within the damaged area. A severity of 0 % is associated with no stiffness degradation whereas a severity of 100 % corresponds to a null stiffness in the damaged area. The input signal is a 5 cycles burst with a central frequency of 100 kHz. To illustrate the influence of

bias and uncertainties in the predictions of a DL model in SHM, we introduce variations between the four models :

$\mathbf{C_0}$ The first one named C_0 has a balanced stacking with 8 layers $[0_2/90_2/+45_2/-45_2]_s$. 100 damage configurations with 3 parameters (two for position and one for severity) are simulated according to Latin Hypercube Sampling.

$\mathbf{C_1}$ A bias and uncertainties on mechanical and geometric properties are introduced in the model of the second structure (Table 2). The unbalanced stack with 10 layers $[0_2/90_2/+45_2/-45_2/0_2]_s$ induces a global anisotropic behavior and uncertainties are added on the mechanical properties, the position of the PZTs and the geometry in order to simulate a batch of coupons in real experimental conditions. The uncertainties take the form of random values added to the values of some geometric or mechanical properties (See Table 2 where $\mathcal{N}_{a,b}$ stands for a gaussian law with mean value a and variance b). The database then contains 80 damage configurations with varying position and severity.

$\mathbf{C_2}$ Imposing strict positioning of the transducers during the fabrication of the structure is not always easy and significant discrepancies can occur between the planned and actual placement. Furthermore, during its lifetime, the transducers network may be damaged or lose some of its elements and be replaced. The third model reproduces that kind of events : the third transducer is positioned differently than in the model C_0 which induces strong variations on the measured signals. The database is composed of 100 damage configurations with varying position and severity.

$\mathbf{C_3}$ The fourth model is similar to the second but the third transducer is also moved. The database then contains 80 damage configurations with varying position and severity.

The labels $\mathbf{C_0}$, $\mathbf{C_1}$, $\mathbf{C_2}$, and $\mathbf{C_3}$ will thus be used throughout the manuscript and will refer to the above defined models. As previously stated, the objectives are here to achieve damage localization and damage severity quantification. Consequently, the damage location over the structure surface will be denotd as x and y and the damage severity will be denoted s in the following in the manuscript.

2.3 Quantification of the difference between cases

To estimate the difference between the previously defined numerical structures, we propose to define Structural Indexes (SI). These SI are defined on the basis of Damage

Table 2: Geometric and mechanical properties of the studied structures

Param.	$\mathbf{C_0}$	$\mathbf{C_1}$	$\mathbf{C_2}$	$\mathbf{C_3}$	Unit
L	500	$500 + \mathcal{N}_{0,2}$	500	$500 + \mathcal{N}_{0,2}$	mm
H	200	$200 + \mathcal{N}_{0,1}$	200	$200 + \mathcal{N}_{0,1}$	mm
PZT 1	$[100, 160]$	$[100, 160] + \mathcal{N}_{\mathbf{0_2},\mathbf{I_2}}$	$[100, 160]$	$[100, 160] + \mathcal{N}_{\mathbf{0_2},\mathbf{I_2}}$	mm
PZT 2	$[100, 40]$	$[100, 40] + \mathcal{N}_{\mathbf{0_2},\mathbf{I_2}}$	$[100, 40]$	$[100, 40] + \mathcal{N}_{\mathbf{0_2},\mathbf{I_2}}$	mm
PZT 3	$[400, 160]$	$[400, 160] + \mathcal{N}_{\mathbf{0_2},\mathbf{I_2}}$	$[400, 40]$	$[400, 40] + \mathcal{N}_{\mathbf{0_2},\mathbf{I_2}}$	mm
E_1	150	$150 + \mathcal{N}_{0,0.5}$	150	$150 + \mathcal{N}_{0,0.5}$	GPa
E_2	9	$9 + \mathcal{N}_{0,0.5}$	9	$9 + \mathcal{N}_{0,0.5}$	GPa
G_{12}	4.7	4.7	4.7	4.7	GPa
ν_{12}	0.33	0.33	0.33	0.33	-
ν_{23}	0.48	0.48	0.48	0.48	-
ρ	1594	1594	1594	1594	kg/m^3
SNR	0	30	0	30	dB
Stacking	ISO	ANISO	ISO	ANISO	-
N_{tr}	80	20	20	20	-
N_{test}	20	60	80	60	-

Indexes (DIs), widely used in SHM to detect damages, but here they compare the healthy signals between different structures instead of signals corresponding to different damage states on a given structure. The underlying idea is that the LWs propagation in healthy structural conditions strongly depends on the structure properties and geometry, so any change (geometry, mechanical properties, sensor positions, etc.) will be caught by those Structural Indexes (SIs). We choose for SI an average of two DIs computed over all the available signals: the Normalized Residual Error (NRE) and the Cross-Correlation (CC) presented in Table 3. The NRE focuses on the energy of the signals while the CC focus on their temporal behavior. For the structures with uncertainties (C_1 and C_3), the SI is the mean of the SIs computed with all the available healthy signals from all coupons.

DI	Definition
CC	$1 - max\left(\frac{IFFT\left[FFT[x_{ij}(t)]FFT[y_{ij}(t)]^*\right]}{\sqrt{(E_{x_{ij}}E_{y_{ij}})}}\right)$
NRE	$\frac{\int_T^0 (x_{ij}(t) - y_{ij}(t))^2 dt}{2 \times \left(\int_T^0 x_{ij}(t)^2 dt + \int_T^0 y_{ij}(t)^2 dt\right)}$

Table 3: Damage Indexes (DIs) used for the computation of Structural Index (SI) with respectively $x_{ij}^s(t)$ and $x_{ij}^t(t)$ the source and target signals for the path between actuator i and sensor j

The resulting SIs are provided in Tab. 4. As expected, the SI obtained by comparing the structure $\mathbf{C_0}$ to itself is equal to 0. When comparing $\mathbf{C_0}$ to $\mathbf{C_1}$ which is the same except that some anisotropy as well as some noise have been added, it can be seen that the resulting SI is rising. $\mathbf{C_2}$ is more different from $\mathbf{C_0}$ as one PZT element is positioned at a slightly different location which results in a increasing value of SI. Finally $\mathbf{C_3}$ is a combination of $\mathbf{C_1}$ and $\mathbf{C_2}$ and consequently exhibits the highest SI value among the

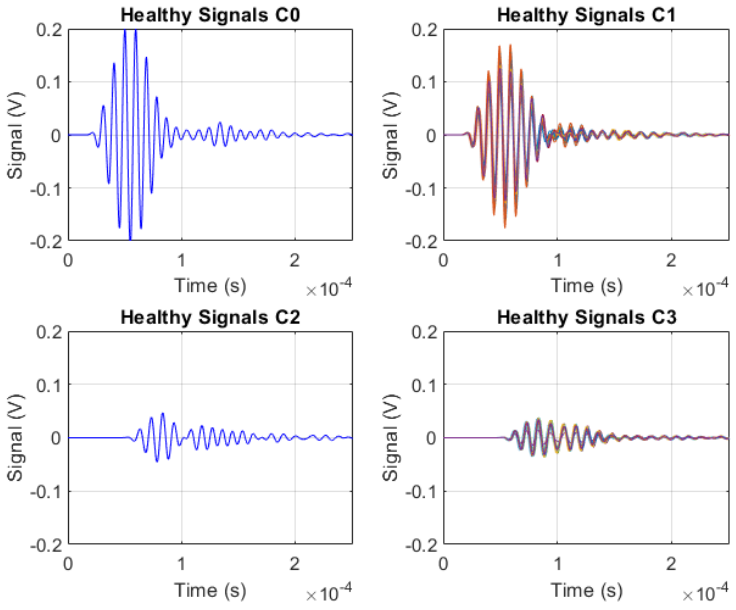

Fig. 5: Healthy signals used to compute the SI (here only signals from actuator 1 to sensor 3 are shown). For structures C_1 and C_3, one different healthy signal for each coupon is present due to the model uncertainties.

four tested numerical cases.

Table 4: Structural Index (SI)

	$\mathbf{C_0 \rightarrow C_0}$	$\mathbf{C_0 \rightarrow C_1}$	$\mathbf{C_0 \rightarrow C_2}$	$\mathbf{C_0 \rightarrow C_3}$
SI	0.0	0.12978	0.5977	0.7466

3 Background on Optimal Transport Theory

The following Section presents the essential results of the optimal transport theory necessary to understand the TL algorithm proposed in this paper. Interested readers may refer to [54] and [52] for more advanced developments as well as further details. Readers interested in the application to LWSHM can jump directly to Section 3.7 for a digest summary of the exposed mathematical developments.

3.1 The Monge problem

The optimal transport problem was described as early as the 18th century by Monge who looked for the most economical solution to move objects from a set of departure points to a set of arrival points. To describe this problem, we consider the source probability measure $\mu \in \mathcal{Z}^s$ and the target probability measure $\nu \in \mathcal{Z}^t$ with the features

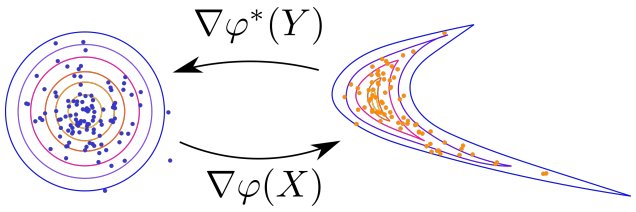

Fig. 6: Transport between two sampled distributions (μ, ν) by the Kantorovich potentials φ and $\overline{\varphi}$.

spaces $\mathcal{Z}^s$ and $\mathcal{Z}^t$. A map T transports the measure μ over the measure ν if for any positive measurable map f we have $\int f\left(T(x)\right) d\mu(x) = \int f(y) d\nu(y)$. The transport is then noted $T_{\#}\mu = \nu$. The cost function $c : \mathcal{Z}^s \times \mathcal{Z}^t \to \mathbb{R}^+$ represents the energy required to move one unit of mass from μ to ν, the total cost to transport with the map T is then given by :

$$C(T) = \int_{\mathcal{Z}^s} c\left(x, T(x)\right) d\mu(x) \tag{2}$$

The minimization of the cost $C(T)$ among all the possible maps T under the constraint $T_{\#}\mu = \nu$ provides the *Optimal Transport Map*.

3.2 The primal Monge-Kantorovich problem

The Monge's problem is relaxed by introducing a joint distribution $\pi \in \Pi(\mu, \nu)$ with respectively μ and ν for the first and second marginals [55]. The problem is no longer described by a function but by a measure called the transport plan. The Wasserstein-2 distance W_2^2 is the optimal transport cost computed with $c(x, y) = \frac{1}{2}\|x - y\|_2^2$ where $\|\cdot\|_2$ denotes the Euclidean norm. The primal Monge-Kantorovich problem then amounts to solve the following optimization:

$$W_2^2(\mu, \nu) = \inf_{\pi \in \Pi(\mu,\nu)} \left[\iint \frac{1}{2}\|x - y\|_2^2 d\pi(x, y) \right] \tag{3}$$

This primal formulation is mathematically advantageous compared to the previous one [54], in particular the existence of a minimum is guaranteed with weak assumptions on the cost function. In [56, 57] the primal problem is solved in a discrete form, leading in that case to a simple linear optimization problem. The minimization of the Sinkhorn distance is achieved very quickly with an entropy regularization exploited in the JDOT [41, 58]. However, in order to transport new samples from one distribution to another - which is required in our approach - the transport plan must be a continuous map.

3.3 The dual Monge-Kantorovich problem

The optimization theory has frequently described the difficulties to solve a problem in its primal formulation and proposes dual formulations to relax it [59]. For the OT, the commonly used Monge-Kantorovich duality introduces two potential functions such as [55]:

$$W_2^2(\mu,\nu) = \sup_{\psi(y)-\varphi(x)\leqslant\frac{1}{2}\|x-y\|_2^2} \left[\int_{\mathcal{Z}^t} \psi(y)d\nu(y) - \int_{\mathcal{Z}^s} \varphi(x)d\mu(x)\right] \tag{4}$$

The Theorem 5.2 in [52] proves that the pair of potential functions $(\varphi,\psi) \in (L^1(\mu) \times L^1(\nu))$ respecting the inequality $\psi(y)-\varphi(x) \leqslant \frac{1}{2}\|x-y\|_2^2$ is a pair of a convex function φ and its conjugate $\overline{\varphi}$. The resolution is then achieved by finding only one convex function:

$$W_2^2(\mu,\nu) = \sup_{\varphi\in \mathrm{CVX}(\mu)} \left[\int \varphi \, d\mu + \int \overline{\varphi} d\nu\right] \tag{5}$$

with: $\overline{\varphi}(y) = \sup_x \left[\frac{1}{2}\|x-y\|_2^2 - \varphi(x)\right]$ the conjugate of φ.

The Theorem 3.3 in [60] shows that the W_2^2 distance is equal to :

$$W_2^2(\mu,\nu) = C_{\mu,\nu} - \inf_{\varphi\in \mathrm{CVX}(\mu))} \left[\int \varphi \, d\mu + \int \overline{\varphi} \, d\nu\right] \tag{6}$$

with: $\overline{\varphi}(y) = \sup_x \left[\langle x,y\rangle - \varphi(x)\right]$ the conjugate (or Legendre transform) of φ,

$C_{\mu,\nu} = \frac{1}{2}\int \|x\|_2^2 d\mu(x) + \frac{1}{2}\int \|y\|_2^2 d\nu(y)$ a constant independent of $(\varphi,\overline{\varphi})$.

3.4 Minimax formulation of the dual Monge-Kantorovich problem

In DL approaches, the densities are generally not accessible and the distributions are sampled. The problem formulated by Equation 6 takes the form of a stochastic optimization on the weights of the model φ by computing the mean of losses with random samples of μ and ν.

$$W_2^2(\mu,\nu) = C_{\mu,\nu} - \inf_{\varphi\in \mathrm{CVX}(\mu)} \left[\mathbb{E}_{x\sim\mu}[\varphi(x)] + \mathbb{E}_{y\sim\nu}\left[\overline{\varphi}(y)\right]\right] \tag{7}$$

In practice, the constraint on the conjugate $\overline{\varphi}(y) = \sup_x \left[\langle x,y\rangle - \varphi(x)\right]$ is not easy to apply. With the help of the Brenier's theorem [61] that remarkably makes the link between

the optimal measure and the optimal convex potential function, the Theorem 3.3 in [60] introduces another convex ψ function such that : $\overline{\varphi}(y) = \sup_{\psi} [\langle y, \nabla\psi(y)\rangle - \varphi(\nabla\psi(y))]$. The problem is then reformulated as a MaxiMin optimisation used in this work:

$$W_2^2(\mu,\nu) = C_{\mu,\nu} + \sup_{\varphi\in \mathrm{CVX}(\mu)} \left[\inf_{\psi\in \mathrm{CVX}(\nu)} [-\mathbb{E}_{x\sim\mu}[\varphi(x)] - \mathbb{E}_{y\sim\nu}[\langle y, \nabla\psi(y)\rangle - \varphi(\nabla\psi(y))]] \right] \tag{8}$$

3.5 Input Convex Neural Network

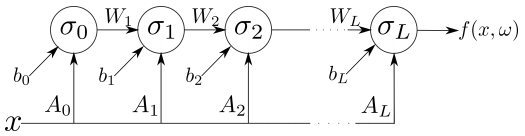

Fig. 7: The Input Convex Neural Network (ICNN) architecture

Input Convex Neural Networks (ICNNs) is a class of neural network whose output is convex with respect to their inputs. Proposed recently in [62], they have known a growing interest thanks to their original properties. They have found applications for classification problems [63], for new control strategies [64] and to approximate the convex functions space [65]. For a given input $x \in \mathbb{R}^d$, the output z_L of the network with L layers of D hidden neurons is defined recursively by the following expression for $i \in [0, 1, .., L]$:

$$z_{i+1} = \sigma_i \left\{ W_i z_i + A_i x + b_i \right\}, \quad h(x,\omega) = z_k \tag{9}$$

with σ_i an activation function, $A_{0:L-1} \in \mathbb{R}^d \times \mathbb{R}^D$ input weight matrices, $W_{1:L-1} \in \mathbb{R}^D \times \mathbb{R}^D$ output weight matrices and $b_{0:L-1} \in \mathbb{R}^D$ bias terms. On the last layer, the weigths are a vector $A_L \in \mathbb{R}^d$, a scalar $W_L \in \mathbb{R}$ and a bias $b_L \in \mathbb{R}$. The function $x \to f(x,\omega)$ is convex with respect to x if [62] : (i) all weights W_i are positive, (ii) the activation function σ_0 is convex and (iii) σ_i is convex and non-decreasing $\forall i \in [1, .., L-1]$. This class of function is rich enough to represent the set of all convex functions [64], the choice of ICNNs to solve the transport problem is then valid.

3.6 Uses of Neural Networks for Kantorovich potentials

The recent advances in DL invite to search the Kantorovich potentials in the form of neural networks to integrate the optimal transport theory to DL methods leading to strong mathematical justifications in the choice of architectures and training loop. The MaxiMin formulation in Equation 8 of the dual problem has been successfully studied

several times. Two ICNN are used to compute simultaneously the potential and its conjugate in [65]. Only one model is trained and the conjugate is computed with the formula of Equation 6. The training can be complex in this approach, the algorithm has been then improved and relaxed in [60] by substituting the conjugate by another ICNN following the results of Equation 8. This proposition is adopted in this work. In [66], the MaxiMin problem is solved with an ICNN as potential and combine it with a generator model inspired by GANs in order to compute the transport between distributions with different dimensions. The MaxiMin problem can also be adapted for distributions with different dimensions and other distances [67].

The distance W_2^2 is particularly popular in a type of generative model, the Wasserstein Generative Adversarial Network (WGAN) [68]. The MaxiMin formulation is used in [69] to enrich a GAN: the Wasserstein distance is computed by solving the dual formulation of the problem with an ANN as potential model. In order to obtain a mathematically explainable generative model, [70] incorporates Kantorovich potentials into the training of a GAN where the discriminator error is the distance W_2^2. The MaxiMin formulation is also used to compute p, q-Wasserstein distances in GAN in [71, 72].

To avoid the difficult task of solving a MaxiMin problem, regularization approaches are interesting alternatives. In [73], the L2 regularization is combined with an entropy regularization based on the values of the potentials. This approach is probably the first to propose to model the Kantorovich potentials by ANNs. In [74], the Wasserstein-2 distance is minimized using a single ICNN combined with a new regularization: the *cycle-consistency* from [75] based on the gradient values of the potentials. This same proposal is exploited for the calculation of Wasserstein barycenters [76]. In [67] the dual problem is used to compute Wasserstein barycenters with ICNN.

3.7 Take away message regarding Optimal Transport

The idea behind optimal transport is therefore to seek the best transformation to perform a mapping between two different spaces through the minimisation of a function evaluating the cost of this transport. In summary, the mathematical developments exposed here are showing that:

- The existence of a minimum of the cost function associated with the optimal transport is guaranteed by making very few assumptions (primal Monge-Kantorovich problem).
- This minimum can be found in the form of a convex function satisfying certain constraints (dual Monge-Kantorovich problem).

- This convex function is accessible in practice via the resolution of an optimization problem of the type MiniMax.
- Input Convex Neural Networks (ICNN) can learn this convex function for optimal transport by learning to solve the optimization problem mentioned in the previous step.

Thus, the solution of the optimal transport problem can be achieved by machine learning and is based on sound mathematical foundations that guarantee the minimization of a relevant cost function.

4 Deep Transfer Learning Implementation

This section then describes the implementation carried out here to illustrate OT in a LWSHM context. The reference CNN on which OT will be applied is first described. Then the implementation of the ICCN performing OT is discussed.

4.1 Reference CNN and input data design

In a LWSHM context, the reference CNN is trained here to estimate the severity and the position of a damage (which corresponds to the task (ii) and (iv) of the SHM process) on a composite structure. The architecture of the reference CNN is inspired from the VGG16 network [16] but adapted for 1D signals. The architecture of the network (Figure 8) is composed of 4 pairs of convolutional layers followed each by a max pooling layer, a normalization layer, a dropout layer and a ReLu activation layer. After the convolutional part of the network, the bottlenecks part is composed of 3 fully connected layers (Table 6). The signals of all the path of actuator-sensors are concatenated to form one input vector (Figure 9) of size 6024. In practice, 3 PZT elements are available, wich leads to a total of 2 possible paths when one of the PZT element is an actuator. This leads to a total of 12 signals of 502 samples that are concatenated together in order to form the desired input vector. The input data are finally normalized between -1 and 1 before being fed to the algorithm.

4.2 OT DT strategy architecture

The Table 6 summarizes the architecture of the OT TL strategy used in this work, as shown inf Fig. 2, and the corresponding hyperparameters are presented Table 5. Two ICNNs of 4 layers of 64 neurons represent the Kantorovich potentials. The choice of this architecture strongly influences the quality of the transport. The same architecture

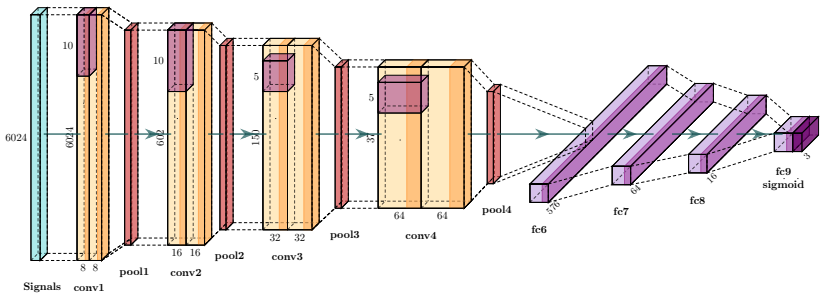

Fig. 8: Architecture of the initial CNN

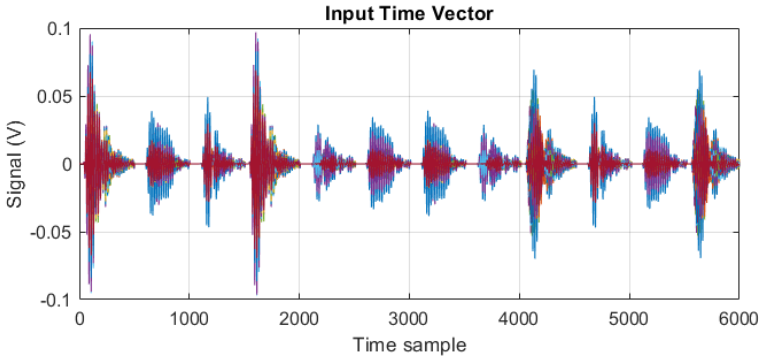

Fig. 9: Inputs of the CNN with all actuator to sensor pathes concatenated in one vector before normalization.

and set of hyperparameters have been used for every case. Their determination relies on empirical knowledge acquired in previous works combined with a trial and error approach.

4.3 Feature extraction and Discriminator training

Even though the ICNNs are theoretically able to transport very high dimension data, the resolution of the transport problem is easier and numerically cheaper with a reduced number of dimensions. The convolutional part f_θ of the CNN in Figure 8 extracts relevant and parsimonious information from the signals. The initial input data size is reduced to 576 after the convolutions. After some fully connected layers only 16 features describes the data. The architecture is summarized in the Table 6. The transport is applied at this intermediate layer at depth $N-2$ by inserting the gradient of the Kantorovich potential. In the formulation of the Equation 6, the distributions are sampled at each iteration. In practice, the densities are not accessible and the number of samples is limited by the

Table 5: Hyperparameters values

Hyperparam.	α	β_s	β_t	t_{iter}	n_{iter}	k_{iter}	j_{iter}	n_s	n_t	lr	lr_φ	lr_ψ
Value	$1e-3$	1	1	1000	1	1	4	80	20	$1e-4$	$0.25e-4$	$0.25e-4$

Table 6: Architectures of the features extractor f_θ, the Kantorovich potential φ_ω and the regressor g_θ

Model	Layer	Parameter	Value
f_θ	Input	size	10040
	Conv1D	Number of filters and filter length	8x10
	Activation	Function	ReLu
	Conv1D	Number of filters and filter length	8x10
	Activation	Function	ReLu
	MaxPool	Window size	10
	Dropout	τ	0.05
	Conv1D	Number of filters and filter length	16x10
	Activation	Function	ReLu
	Conv1D	Number of filters and filter length	16x10
	MaxPool	Window size	4
	Activation	Function	ReLu
	Dropout	τ	0.05
	Conv1D	Number of filters and filter length	32x5
	Activation	Function	ReLu
	Conv1D	Number of filters and filter length	32x5
	Activation	Function	ReLu
	MaxPool	Window size	4
	Conv1D	Number of filters and filter length	32x5
	Conv1D	Number of filters and filter length	32x5
	MaxPool	Window size	4
	Activation	Function	ReLu
	Dropout	τ	0.05
	Dense	Number of hidden neurons	64
	Activation	Function	ReLu
	Dense	Number of hidden neurons	64
	Activation	Function	ReLu
φ_ω	Input Convex Layer	Number of hidden neurons	256
	Input Convex Layer	Number of hidden neurons	64
	Input Convex Layer	Number of hidden neurons	64
	Input Convex Layer	Number of hidden neurons	64
	Input Convex Layer	Number of hidden neurons	1
	∇		
g_θ	Activation	Number of hidden neurons	ReLu
	Dense	Number of hidden neurons	3
	Activation	Function	SoftMax

dataset. To overcome this, the use of dropout layers in the CNN adds variability to each prediction during training.

The Mean Square Error (MSE) between the predicted and the true labels is minimized to train f_θ and g_θ. In addition to this error, the cost function is penalized by the transport cost with the Wasserstein-2 distance W_2^2 to constrain f_θ to extract features common to both target and source domains. Coefficients are introduced to weight each of these errors : β_s and β_t respectively weight the MSE on the source data and on the target data and α weights the influence of the transport cost.

$$\mathcal{L}_\theta = \frac{\beta_s}{n_s}\sum_{i=1}^{n_s}\text{MSE}(\mathcal{M}_\theta^s(x_i^s), y_i^s) + \frac{\beta_t}{n_t}\sum_{j=1}^{n_t}\text{MSE}(\mathcal{M}_\theta^t(x_j^t), y_j^t) + \alpha W_2^2(\nabla\varphi_\omega(f_\theta(x^t), f_\theta(x^s)) \tag{10}$$

4.4 The Dual Monge-Kantorovich problem computation

The two Kantorovich potentials are represented by the ICNNs ψ_γ with weights γ and φ_ω with weights ω. To solve the MaxiMin problem of Equation 8, the training is done in two steps repeated at each iteration. The use of a two-step algorithm for the solution of a MaxiMin problem is usual for the transport problem [60, 66, 73] but also for the training of GAN [77]. Here the first step trains the model ψ_γ to ensure this model is the conjugate of φ_ω and the second step trains φ_ω to compute the transportation between the two domains.

$$\max_{\omega:W_l\geq 0,\forall l\in[L-1]}\ \min_{\gamma:W_l\geq 0,\forall l\in[L-1]} \mathcal{J}_{\omega,\gamma} \tag{11}$$

with :

$$\mathcal{J}_{\omega,\gamma} = \frac{1}{n_t}\sum_{j=1}^{n_t}\varphi_\gamma(\nabla\psi_\omega(z_j^t)) - \langle z_j^t, \nabla\psi_\omega(z_j^t)\rangle - \frac{1}{n_s}\sum_{i=1}^{n_s}\varphi_\gamma(z_i^s) \tag{12}$$

4.5 Global Algorithm

The global training consists in achieving the MaxiMin optimization in 3 steps : first the features extraction model and the discriminative model (f_θ and g_θ) are trained to minimize the loss $\mathcal{L}$ from Equation 10 and then the optimal transport problem is solved by training φ_γ and ψ_ω to minimize $\mathcal{J}$ from Equation 12. The training of φ_γ and ψ_ω follows the optimization loop proposed in Algorithm 1. The global algorithm is not always

Algorithm 1: Dual Monge-Kantorovich problem optimization loop

Input: (μ, ν) source and target distributions; M batch size; T total iterations; φ and ψ : ICNNs with their respective weights ω and γ ;

for $n = 1, .., n_{iter}$ **do**
  for $k = 1, .., k_{iter}$ **do**
    Sample a batch $\{z_j^t\}_{j=1}^{n_t}$ from ν ;
    Update γ to minimize $\frac{1}{n_t}\sum_{j=1}^{n_t} \varphi_\gamma(\nabla\psi_\omega(z_j^t)) - \langle z_j^t, \nabla\psi_\omega(z_j^t)\rangle$;
  for $l = 1, .., l_{iter}$ **do**
    Sample a batch $\{z_i^s\}_{i=1}^{n_s}$ from μ ;
    Update ω to minimize $\frac{1}{n_s}\sum_{i=1}^{n_s} \varphi_\gamma(z_i^s) - \frac{1}{n_s}\sum_{j=1}^{n_t} \varphi_\gamma(\nabla\psi_\omega(z_j^t))$;

easy to train because of its MaxiMin formulation. The different errors and the MaxiMin formulation of the transport problem sometimes make it unstable or do not allow it to converge to an acceptable solution. Several hyperparameters must be optimized: the weights: α, β_s and β_t, the respective learning rates of (f, g), φ and ψ : lr ,lr_φ,lr_ψ, the iteration numbers: t_{iter}, n_{iter}, k_{iter} and j_{iter}, and the size of the batches: n_s and n_t.

Algorithm 2: Deep Transfer Learning with Kantorovich Potentials

Input: $\mathcal{M}_\theta = g_\theta \circ f_\theta$: initial model with f_θ feature model extraction model at layer l and discriminative model g_θ ;
$(\varphi_\omega, \psi_\gamma)$: ICNNs with their respective weights ω and γ;
Data: Set of source data X_s and target data X_t
Output: $\mathcal{M}_\theta^s = g_\theta \circ f_\theta$ and $\mathcal{M}_{\theta,\omega}^t = g_\theta \circ \nabla\varphi_\omega \circ f_\theta$

$\mathcal{M}_{\theta_0}^s \leftarrow g_{\theta_0} \circ f_{\theta_0}$ Initialize source model ;
$\mathcal{M}_{\theta_0,\omega_0}^t \leftarrow g_{\theta_0} \circ \nabla\varphi_{\omega_0} \circ f_{\theta_0}$ Initialize target model ;
for $t = 1, .., t_{iter}$ **do**
  Sample a batch $(x_i^s, y_i^s)_{i=1}^{n_s}$ and $(x_j^t, y_j^t)_{j=1}^{n_t}$ respectively from X^s and X^t ;
  Update θ to minimize $\mathcal{L}_\theta(X_{batch}^s, X_{batch}^t)$ from Equation 10;
  $Z_{batch}^S = \{z_i^s = f_\theta(x_i^s)\}_{i=1}^{n_s}$;
  $Z_{batch}^T = \{z_j^t = f_\theta(x_j^t)\}_{j=1}^{n_t}$;
  Update ω and γ to minimize $\mathcal{J}_{\omega,\gamma}(Z_{batch}^S, Z_{batch}^T)$ from Equation 12 with Algorithm 1

5 Application to LWSHM

5.1 Training and test datasets

We propose here to evaluate the added value of the transfer of the knowledge acquired on the source structure C_0 to the target structures $C_{1\leq i\leq 3}$ in comparison with standard methods which are not performing it. For each of these databases, a part of the samples is used for training and another part is kept for testing the models (see Table 2). In each case during training, 80 samples are used from the source structure C_0 and 20 from the target structures $C_{1\leq i\leq 3}$. N_{tr} represents the number of samples used for training and N_{test} the number of samples kept for testing. For the source domain, this balance of 80 % of data used for training and of 20 % of data used for testing is rather standard and should prevent overfitting. For the the target domain, relying only on 20 % of the data for training and testing on 80 % of the data is much more challenging.

5.2 Performance evaluation

To evaluate the relevance of our TL approach, 4 approaches are compared: a training with only the source data, a training with only the target data and training with source and target data mixed together. In order to quantify the performances of the various methods an integrated Mean Square Error (MSE) has been used. This MSE is the sum of the error in localization for x and y and of the error in severity estimation s. As the localization coordinates are depending on a reference frame and the severity can be null, it was not possible to use here a normalized MSE.

5.2.1 $C_0 \rightarrow C_1$

In this case, the model bias and uncertainties have a slight influence on the performance of the model and the quality of the predictions is not strongly deteriorated. The proposed transfer learning strategy does not bring any clear benefit compared to a simple learning on the source data (see 10 and Figure 11).

5.2.2 $C_0 \rightarrow C_2$

In this case, Figure 13a clearly shows the inability of the model to predict on a structure with a poorly positioned sensor. Figure 13b shows that the number of data in the target domain is insufficient to predict correctly with only target data. The simple approach mixing the two domains does not yield satisfying results because of the strong differences between Input data (Figure 13c). Our TL approach gives a clear improvement

Fig. 10: MSE for the transfer $C_0 \rightarrow C_1$

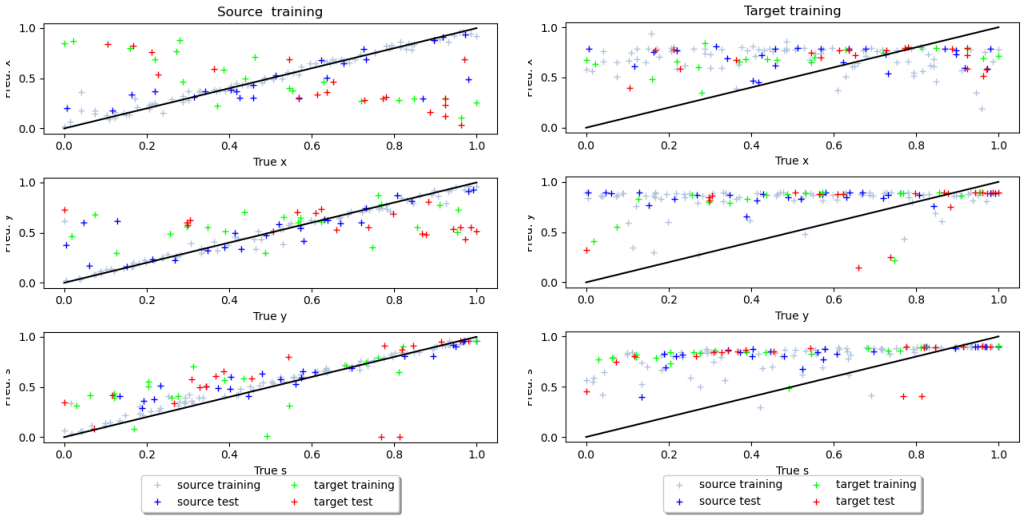

(a) Training with source data

(b) Training with target data

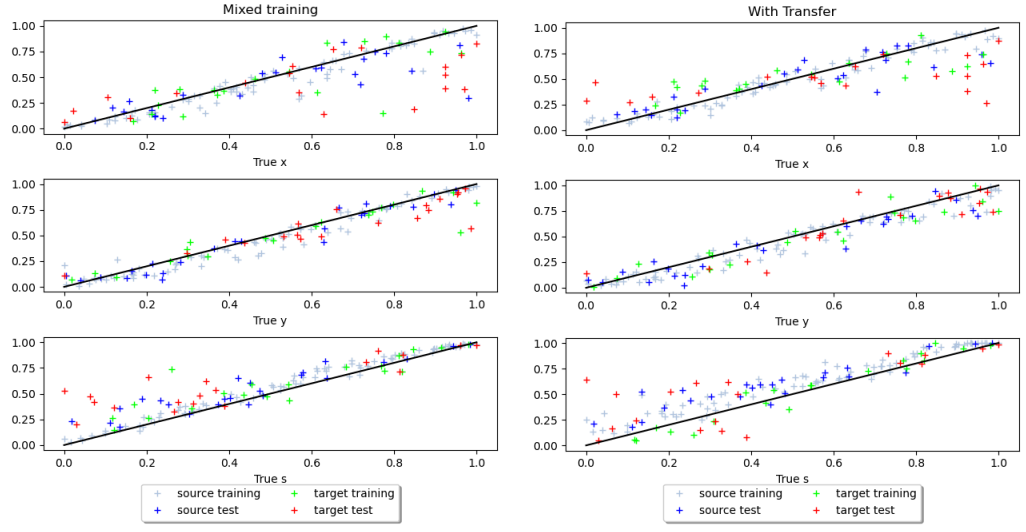

(c) Training without transfert on target and source data

(d) Training with transfer betwen source and target data

Fig. 11: Evaluation of the transfer $C_0 \rightarrow C_1$. The objectives are here to achieve damage localization and damage severity quantification. The damage location over the structure surface will be denoted as x and y and the damage severity is denoted s.

Table 7: Evaluation of our TL methods

(a) MSE on test data from the target domain

	$C_0 \rightarrow C_0$	$C_0 \rightarrow C_1$	$C_0 \rightarrow C_2$	$C_0 \rightarrow C_3$
Source only	**0.047**	**0.047**	0.161	0.165
Target only	-	0.103	0.101	0.120
Mixed data	-	0.057	0.083	0.121
Our Transfer	-	0.053	**0.033**	**0.051**

(b) MSE on test data from the source domain

	$C_0 \rightarrow C_0$	$C_0 \rightarrow C_1$	$C_0 \rightarrow C_2$	$C_0 \rightarrow C_3$
Source only	**0.0163**	**0.0163**	0.033	0.026
Target only	-	0.063	0.150	0.151
Mixed data	-	0.0195	0.0173	**0.025**
Our Transfer	-	0.0194	**0.0133**	0.036

of the predictions with an reduction of more than 50% of the prediction error on the target data (Figure 13d).

5.2.3 $C_0 \rightarrow C_3$

The results of this last case are very similar to those of the previous one, Figure 15a shows the difficulties of the model to predict on a structure with a badly positioned sensor and Figure 14 shows that the transfer learning approach proposed here decreases by more than 50% the prediction error on the target data.

5.3 Performances overview

Table 7b and Table 7a compare the different approaches evaluated respectively on the source and target domain with test data. Our approach reduces the prediction error of the structures by almost 50% when the differences between the structures are relatively strong. For structures that are close with small SI, our approach does not bring any benefit. Figure 16 compares the evolution of the errors for the different methods as a function of the SI. While the error of the approaches without transfer data rises with the SI, our transfer approach maintains the error at a low level.

The blue curves in the Figure 16 shows that the accuracy of the CNN trained with the C_0 data decrease while the SI rise. With small variations on the structure such as uncertainties ($C_0 \rightarrow C_1$), the Mean Squared Error (MSE) of the predictions is still low but with a change in one PZT position in the model ($C_0 \rightarrow C_2$ and $C_0 \rightarrow C_3$) the accuracy decreases strongly. The CNN is unable to characterize correctly a damage when significant differences exist between the structures, a new approach based on TL is thus required to generalize the knowledge of the DL models.

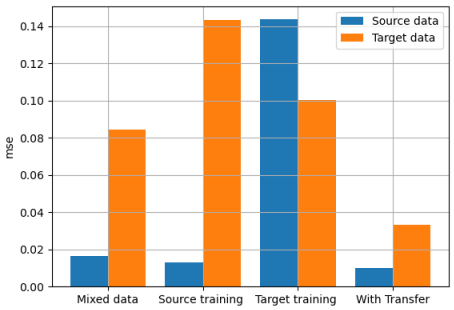

Fig. 12: MSE for the transfer $C_0 \rightarrow C_2$

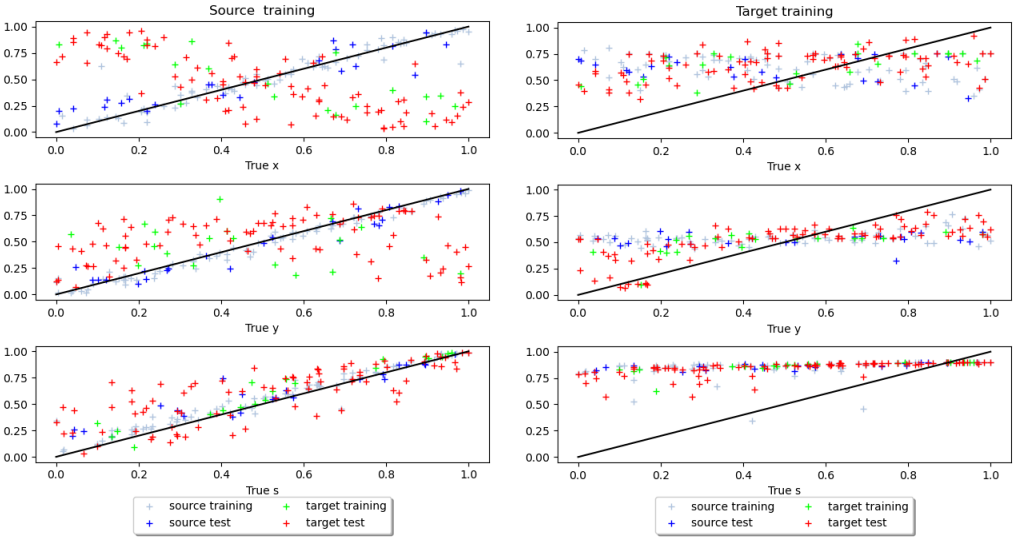

(a) Training on source data

(b) Training with target data

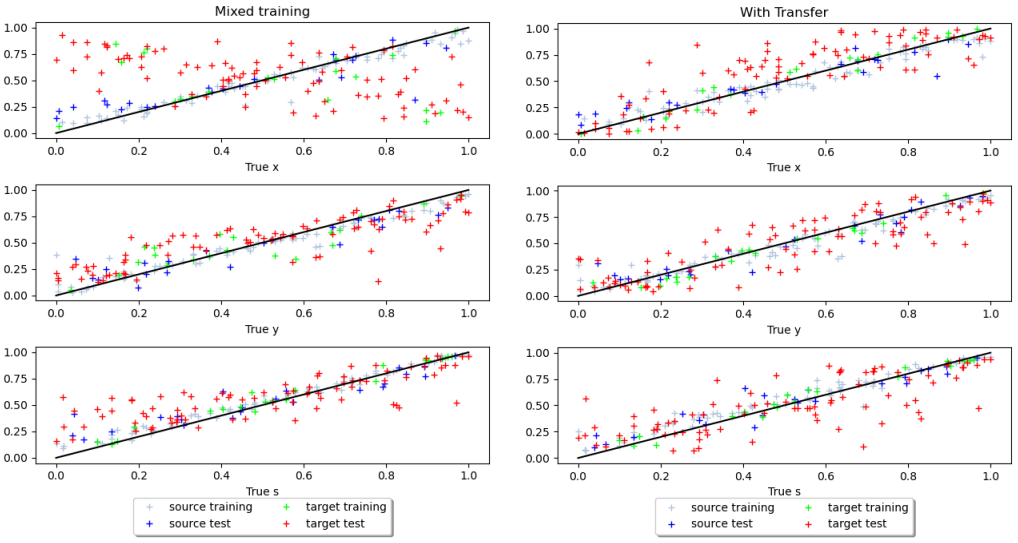

(c) Trainig without transfert on target and source data

(d) Training with transfer betwen source and target data

Fig. 13: Evaluation of the transfer $C_0 \rightarrow C_2$. The objectives are here to achieve damage localization and damage severity quantification. The damage location over the structure surface will be denoted as x and y and the damage severity is denoted s.

Fig. 14: MSE for the transfer $C_0 \rightarrow C_3$

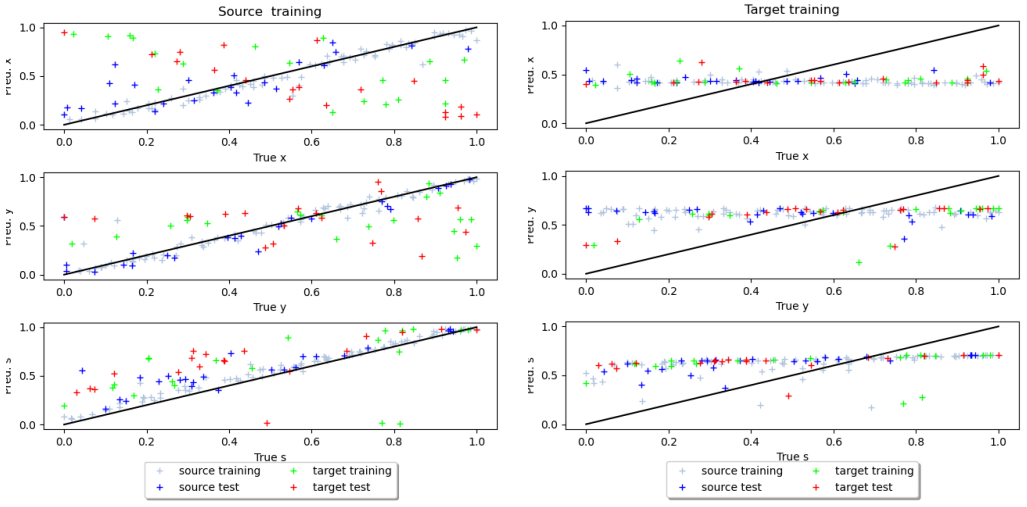

(a) Training on source data

(b) Training with target data

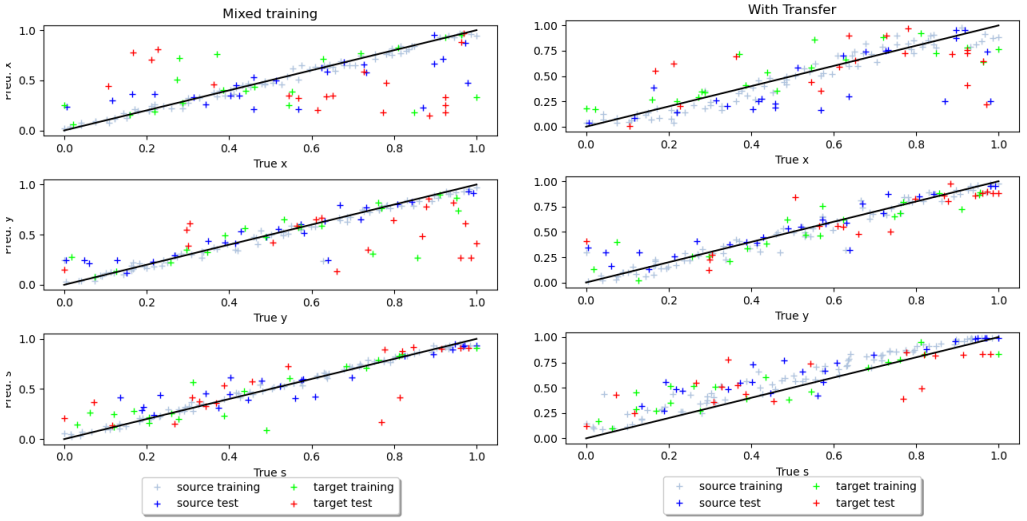

(c) Training without transfer on target and source data

(d) Training with transfer between source and target data

Fig. 15: Evaluation of the transfer $C_0 \rightarrow C_3$. The objectives are here to achieve damage localization and damage severity quantification. The damage location over the structure surface will be denoted as x and y and the damage severity is denoted s.

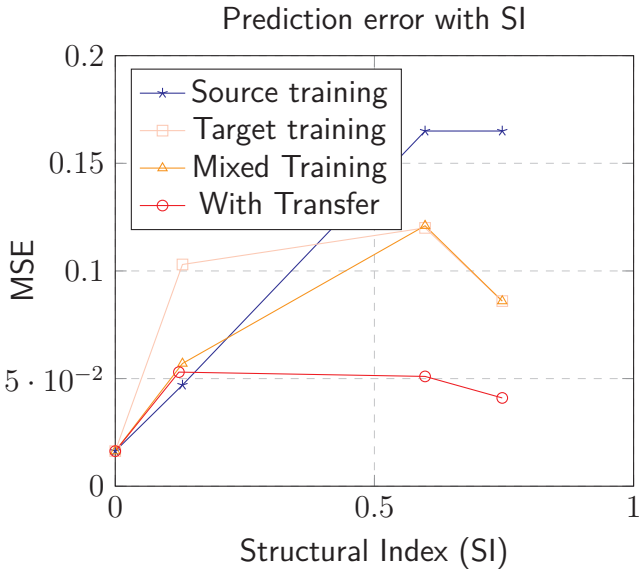

Fig. 16: Prediction error evolution with SI for the different tested TL approaches

6 Discussion

6.1 Advantages and limitations

It is shown here in a LWSHM context that the solution of the optimal transport problem can be achieved by machine learning and is based on sound mathematical foundations that guarantee the minimization of a relevant cost function. Compared to the TCA, JDA and ARTL methods, the optimal transport based methods do not make any assumption about the underlying nonlinear transformation to be applied but discovers it via learning an ICNN network. This potentially leads to better generalization properties and potentially relies on much less data than traditional mapping based TL approaches. Furthermore, as the proposed strategy relies on an ICNN, it integrates naturally within any ML frameworks or algorithms.

The CNN used here extracts automatically abstract features from the data. Only a small SHM expertise is thus necessary and the proposed algorithm is relatively standard for any type of data. Further works can focus on the integration of SHM knowledge in the algorithm to facilitate the training and custom the architectures. Especially, only a few hypothesis are done on the cost function chosen here in the statement of the dual Monge-Kantorovich problem. The research of a cost more specific to the SHM could be an interesting perspective.

Nevertheless, the proposed approach is still a data-based approach and consequently, a certain amount of data is still mandatory in order to train the various ML algorithms involved here. It is also important to mention that the training phase is particularly

tricky and that finding hyperparameters providing correct results can be difficult. Consequently, upcoming work dedicated to make the proposed approach more robust by automatically finding adequate hyperparrameters, or at least by providing a range in which hyperparameters should be selected, should be achieved.

6.2 Closing the gab between academy and industry

Despite an important research effort on LWSHM, there is however relatively few routine industrial applications. Reasons for the slow transfer include among other insufficient attention to how the large data flows will be handled and the lack of performance validation on real structures in industrial environments. The work presented here is thus a potential part of the solution to bridge the gap between academy and industry in the LWSHM context. However, the damage model we used is very simple and reproduces incompletely the effect of a real damage. The TL approach proposed here could also be used to correct the effects of a poor damage modelling. The approach can indeed now be applied more largely to open experimental datasets dedicated to LWSHM such as the OpenguidedWaves[1] one or the REMAP one[2] for example among others. Such datasets contains measurements performed on similar composite structures equipped with piezoelectric elements and monitored by LWs. Consequently, one of the experimentally tested structure can be used to train the initial CNN. Afterwards OT DL strategy can be tested by assessing how TL can be efficiently achieved between the structure used for training and the other experimental structures. This will help in demonstrating from an industrial perspective the relevance of the proposed approach.

Furthermore, the SI defined here is a relevant index to determine the structural proximity between two structures. Our choice of SI is based on empirical knowledge acquired with the DIs used in damage detection. Further work will focus on the computation of other SIs to find the best formula and will apply it on other cases to determine an adequate threshold. An ideal SI should be unique for any kind of structure in order to determine in advance if a transfer strategy is necessary or not with a new dataset. The previously mentioned databases can help in doing so and in transferring the proposed approach toward industrial applications.

6.3 Limiting the experimental needs

Finally, this work opens the way to hybrid models mixing large numerical dataset with small and costly experimental dataset for LWSHM. Using the proposed approach,

[1] http://openguidedwaves.de/
[2] https://dataverse.nl/dataverse/ReMAP_H2020_SHM_data_repository

real applications based on DL can be targeted faster with fewer data and the proposed approach will naturally integrates the variability between aeronautic structures. The proposed approach indeed allows to use only a reduced number of simulations to train a DL model on a new structure globally, but not exaclty, similar to a previous one. This considerably reduces the computation time required for the generation of dataset and for algorithms learning in LWSHM. The validity of such an approach still needs to be demonstrated but theoretically, numerical models seem to be close enough to experimental data to guarantee that such an attempt would be successful.

7 Conclusion

In Lamb Waves based Structural Health Monitoring (LWSHM) of composite aeronautic structures, Deep Learning (DL) methods have proven to be promising to monitor damage using the signals collected by piezoelectric sensors (PZTs). However, those data driven algorithms are strongly problem dependent: any structural change dramatically impacts the accuracy of the predictions and the generalization of the learnt algorithms to other structures within the fleet is impossible. Transfer Learning (TL) promises to face that issue by capitalizing on the knowledge acquired on a given structure to transfer it on another from the fleet. An original TL approach based on the Optimal Transport (OT) theory is proposed here to handle this issue. OT provides a rigorous mathematical framework for TL that can be practically implemented using Input Convex Neural Networks modelling Kantorovich potentials but that has never been used for LWSHM. Using OT, the knowledge acquired on a rich LW database is transferred to poorer LW databases collected on different structures with rising structural divergences. A Structural Index (SI) is defined and used to compute the gap between those different structures and can be used to estimate a priori the necessity of the use of TL methods. The proposed OT based TL method for LWSHM manages to reduce by almost 50% the predictions errors between numerical structures with strong differences (bias in mechanical properties and erroneous PZT position) in comparison with standard approaches. That leads to a promising approach to combine rich numerical database with poorer database in order to build robust algorithms for LWSHM of a fleet of aeronautical composite structures.

Authors' Contributions

Postorino Hadrien defined the numerical case studies, generated the datasets, implemented and evaluated the proposed algorithms. Monteiro Eric reviewed the numerical models. All authors reviewed the final manuscript.

References

[1] V. Giurgiutiu. Structural health monitoring of aerospace composites. Elsevier, Amsterdam, 2016. ISBN 978-0-12-409605-9.

[2] H. Lamb. On waves in an elastic plate. Proceedings of the Royal Society of London. Series A, Containing Papers of a Mathematical and Physical Character, 93(648):114–128, March 1917. doi:10.1098/rspa.1917.0008. Publisher: Royal Society.

[3] S. Guo, M. Rébillat, and N. Mechbal. Dichotomy property of dispersion equation of guided waves propagating in anisotropic composite plates. Mechanical Systems and Signal Processing, 164, 2022.

[4] S. Guo, M. Rébillat, and N. Mechbal. Prediction of frequency and spatially dependent attenuation of guided waves propagating in mounted and unmounted a380 parts made up of anisotropic viscoelastic composite laminates. Structural Health Monitoring, 2022.

[5] S. Gopalakrishnan, M. Ruzzene, and S. Hanagud. Computational Techniques for Structural Health Monitoring. Springer Series in Reliability Engineering. Springer London, London, 2011. ISBN 978-0-85729-283-4 978-0-85729-284-1. doi:10.1007/978-0-85729-284-1.

[6] H. Yun, R. Rayhana, S. Pant, M. Genest, and Z. Liu. Nonlinear ultrasonic testing and data analytics for damage characterization: A review. Measurement, 186:110155, December 2021. ISSN 02632241. doi:10.1016/j.measurement.2021.110155.

[7] A. Rytter. Vibrational Based Inspection of Civil Engineering Structures. PhD thesis, Dept. of Building Technology and Structural Engineering, Aalborg University, 1993.

[8] M. Rébillat, O. Hmad, F. Kadri, and N. Mechbal. Peaks over threshold–based detector design for structural health monitoring: Application to aerospace structures. Structural Health Monitoring, 17(1):91–107, 2018.

[9] A. Rahbari, M. Rébillat, N. Mechbal, and S. Canu. Unsupervised damage clustering in complex aeronautical composite structures monitored by lamb waves: An inductive approach. Engineering Applications of Artificial Intelligence, 97, 2021.

[10] C. Fendzi, N. Mechbal, M. Rebillat, M. Guskov, and G. Coffignal. A general bayesian framework for ellipse-based and hyperbola-based damage localization in anisotropic composite plates. Journal of Intelligent Material Systems and Structures, 27(3):350–374, 2016.

[11] C. Fendzi, M. Rébillat, N. Mechbal, M. Guskov, and G. Coffignal. A data-driven temperature compensation approach for Structural Health Monitoring using Lamb waves. Structural Health Monitoring, 15(5):525–540, September 2016. ISSN 1475-9217. doi:10.1177/1475921716650997. Publisher: SAGE Publications.

[12] M. Rébillat and N. Mechbal. Damage localization in geometrically complex aeronautic structures using canonical polyadic decomposition of lamb wave difference signal tensors. Structural Health Monitoring, 19(1):305–321, 2020.

[13] M. Ghrib, M. Rébillat, G. V. Des Roches, and N. Mechbal. Automatic damage type classification and severity quantification using signal based and nonlinear model based damage sensitive features. Journal of Process Control, 83:136–146, 2019.

[14] W. Briand, M. Rébillat, M. Guskov, and N. Mechbal. Upcoming damage size quantification in aeronautic composite structures based on imaging results post-processing. Journal of Intelligent Material Systems and Structures, 30(2), 2021.

[15] N. Yue, A. Broer, W. Briand, M. Rébillat, T. Loutas, et al. Assessing stiffness degradation of stiffened composite panels in post-buckling compression-compression fatigue using guided waves. Composite Structures, 293:115751, 2022. ISSN 0263-8223.

[16] K. Simonyan and A. Zisserman. Very Deep Convolutional Networks for Large-Scale Image Recognition. arXiv:1409.1556 [cs], April 2015, URL http://arxiv.org/abs/1409.1556. arXiv: 1409.1556.

[17] S. Abdoli, P. Cardinal, and A. Lameiras Koerich. End-to-end environmental sound classification using a 1D convolutional neural network. Expert Systems with Applications, 136:252–263, December 2019. ISSN 0957-4174. doi:10.1016/j.eswa.2019.06.040.

[18] R. Wang, Chencho, S. An, J. Li, L. Li, et al. Deep residual network framework for structural health monitoring. Structural Health Monitoring, 20(4):1443–1461, July 2021. ISSN 1475-9217, 1741-3168. doi:10.1177/1475921720918378.

[19] V. Ewald, R. M. Groves, and R. Benedictus. DeepSHM: A deep learning approach for structural health monitoring based on guided lamb wave technique. In Sensors and Smart Structures Technologies for Civil, Mechanical, and Aerospace Systems 2019, volume 10970, pages 84–99. SPIE, 2019.

[20] I. Tabian, H. Fu, and Z. Sharif Khodaei. Impact Detection on Composite Plates Based on Convolution Neural Network. Key Engineering Materials, 827:476–481, December 2019. ISSN 1662-9795. doi:10.4028/www.scientific.net/KEM.827.476.

[21] L. Xu, Y. Qingyun, Q. Chen, and J. Ren. Guided Wave-Convolutional Neural Network Based Fatigue Crack Diagnosis of Aircraft Structures. Sensors, 19:3567, August 2019. doi:10.3390/s19163567.

[22] H. Zhang, J. Lin, J. Hua, and T. Tong. Interpretable convolutional sparse coding method of Lamb waves for damage identification and localization. Structural Health Monitoring, page 14759217211044806, October 2021. ISSN 1475-9217. doi:10.1177/14759217211044806. Publisher: SAGE Publications.

[23] P. Pandey, A. Rai, and M. Mitra. Explainable 1-D convolutional neural network for damage detection using Lamb wave. Mechanical Systems and Signal Processing, 164: 108220, February 2022. ISSN 08883270. doi:10.1016/j.ymssp.2021.108220.

[24] N. Lu and T. Yin. Transferable common feature space mining for fault diagnosis with imbalanced data. Mechanical Systems and Signal Processing, 156:107645, July 2021. ISSN 08883270. doi:10.1016/j.ymssp.2021.107645.

[25] B. Yang, Y. Lei, F. Jia, N. Li, and Z. Du. A Polynomial Kernel Induced Distance Metric to Improve Deep Transfer Learning for Fault Diagnosis of Machines. IEEE Transactions on Industrial Electronics, 67(11):9747–9757, November 2020. ISSN 0278-0046, 1557-9948. doi:10.1109/TIE.2019.2953010.

[26] M. de Oliveira, A. Monteiro, and J. Vieira Filho. A New Structural Health Monitoring Strategy Based on PZT Sensors and Convolutional Neural Network. Sensors, 18(9): 2955, September 2018. ISSN 1424-8220. doi:10.3390/s18092955.

[27] R. Cui, G. Azuara, F. Lanza di Scalea, and E. Barrera. Damage imaging in skin-stringer composite aircraft panel by ultrasonic-guided waves using deep learning with convolutional neural network. Structural Health Monitoring, page 147592172110239, June 2021. ISSN 1475-9217, 1741-3168. doi:10.1177/14759217211023934.

[28] L. Bull, P. Gardner, J. Gosliga, T. Rogers, N. Dervilis, et al. Foundations of population-based SHM, Part I: Homogeneous populations and forms. Mechanical Systems and Signal Processing, 148:107141, February 2021. ISSN 08883270. doi:10.1016/j.ymssp.2020.107141.

[29] M. Rautela and S. Gopalakrishnan. Ultrasonic guided wave based structural damage detection and localization using model assisted convolutional and recurrent neural networks. Expert Systems with Applications, 167:114189, April 2021. ISSN 0957-4174. doi:10.1016/j.eswa.2020.114189.

[30] C. Su, M. Jiang, S. Lv, S. Lu, L. Zhang, et al. Improved Damage Localization and Quantification of CFRP Using Lamb Waves and Convolution Neural Network. IEEE Sensors Journal, 19(14):5784–5791, July 2019. ISSN 1530-437X, 1558-1748, 2379-9153. doi:10.1109/JSEN.2019.2908838.

[31] A. Kulakovskyi. Développement d'un système SHM pour aéronef par ondes élastiques guidées. PhD thesis, École Polytechnique, 2019, URL http://www.theses.fr/2019SACLX021/document.

[32] S. Zhang, C. M. Li, and W. Ye. Damage localization in plate-like structures using time-varying feature and one-dimensional convolutional neural network. Mechanical Systems and Signal Processing, 147:107107, January 2021. ISSN 0888-3270. doi:10.1016/j.ymssp.2020.107107.

[33] P. Gardner, L. Bull, J. Gosliga, N. Dervilis, and K. Worden. Foundations of population-based SHM, Part III: Heterogeneous populations – Mapping and transfer. Mechanical Systems and Signal Processing, 149:107142, February 2021. ISSN 08883270. doi:10.1016/j.ymssp.2020.107142.

[34] M. Rautela and S. Gopalakrishnan. Deep learning frameworks for wave propagation-based damage detection in 1d-waveguides. In Proceedings of 11th International Symposium on NDT in Aerospace, volume 2, pages 1–11, 2019.

[35] K. Weiss, T. M. Khoshgoftaar, and D. Wang. A survey of transfer learning. Journal of Big Data, 3(1):9, December 2016. ISSN 2196-1115. doi:10.1186/s40537-016-0043-6. Number: 1.

[36] S. J. Pan and Q. Yang. A Survey on Transfer Learning. IEEE Transactions on Knowledge and Data Engineering, 22(10):1345–1359, October 2010. ISSN 1041-4347. doi:10.1109/TKDE.2009.191. Number: 10.

[37] C. Tan, F. Sun, T. Kong, W. Zhang, C. Yang, et al. A Survey on Deep Transfer Learning. arXiv:1808.01974 [cs, stat], August 2018, URL http://arxiv.org/abs/1808.01974. arXiv: 1808.01974.

[38] M. Long, J. Wang, G. Ding, J. Sun, and P. S. Yu. Transfer Feature Learning with Joint Distribution Adaptation. In 2013 IEEE International Conference on Computer Vision, pages 2200–2207, Sydney, Australia, December 2013. IEEE. ISBN 978-1-4799-2840-8. doi:10.1109/ICCV.2013.274.

[39] T. Han, C. Liu, W. Yang, and D. Jiang. Deep transfer network with joint distribution adaptation: A new intelligent fault diagnosis framework for industry application. ISA Transactions, 97:269–281, February 2020. ISSN 0019-0578. doi:10.1016/j.isatra.2019.08.012.

[40] B. Zhang, X. Hong, and Y. Liu. Distribution adaptation deep transfer learning method for cross-structure health monitoring using guided waves. Structural Health Monitoring, page 147592172110107, May 2021. ISSN 1475-9217, 1741-3168. doi:10.1177/14759217211010709.

[41] B. B. Damodaran, B. Kellenberger, R. Flamary, D. Tuia, and N. Courty. DeepJDOT: Deep Joint Distribution Optimal Transport for Unsupervised Domain Adaptation. arXiv:1803.10081 [cs], September 2018, URL http://arxiv.org/abs/1803.10081. arXiv: 1803.10081.

[42] P. Gardner, L. Bull, N. Dervilis, and K. Worden. Overcoming the problem of repair in structural health monitoring: Metric-informed transfer learning. Journal of Sound and Vibration, page 116245, June 2021. ISSN 0022460X. doi:10.1016/j.jsv.2021.116245.

[43] S. J. Pan, I. W. Tsang, J. T. Kwok, and Q. Yang. Domain Adaptation via Transfer Component Analysis. IEEE Transactions on Neural Networks, 22(2):199–210, February 2011. ISSN 1045-9227, 1941-0093. doi:10.1109/TNN.2010.2091281.

[44] T. G. Ritto, K. Worden, D. J. Wagg, F. A. Rochinha, and P. Gardner. A transfer learning-based digital twin for detecting localised torsional friction in deviated wells. Mechanical Systems and Signal Processing, 173:109000, July 2022. ISSN 0888-3270. doi:10.1016/j.ymssp.2022.109000.

[45] Z. Zhang, C. Sun, and B. Guo. Transfer-learning guided Bayesian model updating for damage identification considering modeling uncertainty. Mechanical Systems and Signal Processing, 166:108426, March 2022. ISSN 0888-3270. doi:10.1016/j.ymssp.2021.108426.

[46] Y. Li, T. Bao, Z. Gao, X. Shu, K. Zhang, et al. A new dam structural response estimation paradigm powered by deep learning and transfer learning techniques. Structural Health Monitoring, page 147592172110097, May 2021. ISSN 1475-9217, 1741-3168. doi:10.1177/14759217211009780.

[47] S.-X. Chen, L. Zhou, Y.-Q. Ni, and X.-Z. Liu. An acoustic-homologous transfer learning approach for acoustic emission–based rail condition evaluation. Structural

Health Monitoring, 20(4):2161–2181, July 2021. ISSN 1475-9217, 1741-3168. doi:10.1177/1475921720976941.

[48] C. Feng, H. Zhang, S. Wang, Y. Li, H. Wang, et al. Structural Damage Detection using Deep Convolutional Neural Network and Transfer Learning. KSCE Journal of Civil Engineering, 23(10):4493–4502, October 2019. ISSN 1976-3808. doi:10.1007/s12205-019-0437-z.

[49] E. Tzeng, J. Hoffman, K. Saenko, and T. Darrell. Adversarial Discriminative Domain Adaptation. arXiv:1702.05464 [cs], February 2017, URL http://arxiv.org/abs/1702.05464. arXiv: 1702.05464.

[50] M. Long, Z. Cao, J. Wang, and M. I. Jordan. Conditional Adversarial Domain Adaptation. Technical Report arXiv:1705.10667, arXiv, December 2018, URL http://arxiv.org/abs/1705.10667. arXiv:1705.10667 [cs] type: article.

[51] J. Gosliga, P. Gardner, L. Bull, N. Dervilis, and K. Worden. Foundations of Population-based SHM, Part II: Heterogeneous populations – Graphs, networks, and communities. Mechanical Systems and Signal Processing, 148:107144, February 2021. ISSN 08883270. doi:10.1016/j.ymssp.2020.107144.

[52] C. Villani. Optimal transport: old and new. Number 338 in Grundlehren der mathematischen Wissenschaften. Springer, Berlin, 2009. ISBN 978-3-540-71049-3. OCLC: ocn244421231.

[53] E. Balmes and A. Deraemaeker. Modeling structures with piezoelectric materials. Theory and SDT tutorial. SDTools, Paris, France, September 2013, URL http://www.sdtools.com/help/piezo.pdf.

[54] L. Ambrosio and N. Gigli. A User's Guide to Optimal Transport. In Modelling and Optimisation of Flows on Networks, volume 2062, pages 1–155. Springer Berlin Heidelberg, Berlin, Heidelberg, 2013. ISBN 978-3-642-32159-7 978-3-642-32160-3, URL http://link.springer.com/10.1007/978-3-642-32160-3_1. Series Title: Lecture Notes in Mathematics.

[55] L. Kantorovitch. On the Translocation of Masses. Management Science, 5(1):1–4, 1958, URL http://www.jstor.org/stable/2626967.

[56] M. Cuturi. Sinkhorn Distances: Lightspeed Computation of Optimal Transportation Distances. arXiv:1306.0895 [stat], June 2013, URL http://arxiv.org/abs/1306.0895. arXiv: 1306.0895.

[57] R. Flamary, N. Courty, A. Gramfort, M. Z. Alaya, A. Boisbunon, et al. POT: Python Optimal Transport. Journal of Machine Learning Research, 22(78):1–8, 2021. ISSN 1533-7928, URL http://jmlr.org/papers/v22/20-451.html.

[58] N. Courty, R. Flamary, A. Habrard, and A. Rakotomamonjy. Joint Distribution Optimal Transportation for Domain Adaptation. arXiv:1705.08848 [cs, stat], October 2017, URL http://arxiv.org/abs/1705.08848. arXiv: 1705.08848.

[59] S. P. Boyd and L. Vandenberghe. Convex optimization. Cambridge University Press, Cambridge, UK ; New York, 2004. ISBN 978-0-521-83378-3.

[60] A. Makkuva, A. Taghvaei, S. Oh, and J. Lee. Optimal transport mapping via input convex neural networks. In Proceedings of the 37th International Conference on Machine Learning, pages 6672–6681. PMLR, November 2020, URL https://proceedings.mlr.press/v119/makkuva20a.html. ISSN: 2640-3498.

[61] Y. Brenier. Polar factorization and monotone rearrangement of vector-valued functions. Communications on Pure and Applied Mathematics, 44(4): 375–417, 1991. ISSN 1097-0312. doi:10.1002/cpa.3160440402. _eprint: https://onlinelibrary.wiley.com/doi/pdf/10.1002/cpa.3160440402.

[62] B. Amos, L. Xu, and J. Z. Kolter. Input Convex Neural Networks. arXiv:1609.07152 [cs, math], June 2017, URL http://arxiv.org/abs/1609.07152. arXiv: 1609.07152.

[63] S. Sivaprasad, A. Singh, N. Manwani, and V. Gandhi. The Curious Case of Convex Neural Networks. arXiv:2006.05103 [cs, stat], July 2021, URL http://arxiv.org/abs/2006.05103. arXiv: 2006.05103.

[64] Y. Chen, Y. Shi, and B. Zhang. Optimal Control Via Neural Networks: A Convex Approach. arXiv:1805.11835 [math], February 2019, URL http://arxiv.org/abs/1805.11835. arXiv: 1805.11835.

[65] A. Taghvaei and A. Jalali. 2-Wasserstein Approximation via Restricted Convex Potentials with Application to Improved Training for GANs. arXiv:1902.07197 [cs, math, stat], February 2019, URL http://arxiv.org/abs/1902.07197. arXiv: 1902.07197.

[66] L. Rout, A. Korotin, and E. Burnaev. Generative Modeling with Optimal Transport Maps. arXiv:2110.02999 [cs], October 2021, URL http://arxiv.org/abs/2110.02999. arXiv: 2110.02999.

[67] J. Fan, S. Liu, S. Ma, Y. Chen, and H. Zhou. Scalable Computation of Monge Maps with General Costs. Technical Report arXiv:2106.03812, arXiv, November 2021, URL http://arxiv.org/abs/2106.03812. arXiv:2106.03812 [cs, math] type: article.

[68] M. Arjovsky, S. Chintala, and L. Bottou. Wasserstein GAN. arXiv:1701.07875 [cs, stat], December 2017, URL http://arxiv.org/abs/1701.07875. arXiv: 1701.07875.

[69] N. Dam, Q. Hoang, T. Le, T. D. Nguyen, H. Bui, et al. Three-Player Wasserstein GAN via Amortised Duality. In Proceedings of the Twenty-Eighth International Joint Conference on Artificial Intelligence, pages 2202–2208, Macao, China, August 2019. International Joint Conferences on Artificial Intelligence Organization. ISBN 978-0-9992411-4-1. doi:10.24963/ijcai.2019/305.

[70] J. Leygonie, J. She, A. Almahairi, S. Rajeswar, and A. Courville. Adversarial Computation of Optimal Transport Maps. arXiv:1906.09691 [cs, stat], June 2019, URL http://arxiv.org/abs/1906.09691. arXiv: 1906.09691.

[71] A. Mallasto, J. Frellsen, W. Boomsma, and A. Feragen. (q,p)-Wasserstein GANs: Comparing Ground Metrics for Wasserstein GANs, February 2019, URL http://arxiv.org/abs/1902.03642. Number: arXiv:1902.03642 arXiv:1902.03642 [cs, stat].

[72] Y. Chen, M. Telgarsky, C. Zhang, B. Bailey, D. Hsu, et al. A Gradual, Semi-Discrete Approach to Generative Network Training via Explicit Wasserstein Minimization. In Proceedings of the 36th International Conference on Machine Learning, pages 1071–1080. PMLR, May 2019, URL https://proceedings.mlr.press/v97/chen19h.html. ISSN: 2640-3498.

[73] V. Seguy, B. B. Damodaran, R. Flamary, N. Courty, A. Rolet, et al. Large-Scale Optimal Transport and Mapping Estimation. In ICLR 2018 - International Conference on Learning Representations, pages 1–15, Vancouver, Canada, April 2018. URL https://hal.inria.fr/hal-01956354.

[74] A. Korotin, V. Egiazarian, A. Asadulaev, A. Safin, and E. Burnaev. Wasserstein-2 Generative Networks. In arXiv preprint, September 2020, URL https://openreview.net/forum?id=bEoxzW_EXsa.

[75] J.-Y. Zhu, T. Park, P. Isola, and A. A. Efros. Unpaired Image-to-Image Translation Using Cycle-Consistent Adversarial Networks. In 2017 IEEE International Conference on Computer Vision (ICCV), pages 2242–2251, October 2017. doi:10.1109/ICCV.2017.244. ISSN: 2380-7504.

[76] A. Korotin, L. Li, J. Solomon, and E. Burnaev. Continuous Wasserstein-2 Barycenter Estimation without Minimax Optimization. Technical Report arXiv:2102.01752, arXiv, February 2021, URL http://arxiv.org/abs/2102.01752. arXiv:2102.01752 [cs, stat] type: article.

[77] I. Goodfellow, J. Pouget-Abadie, M. Mirza, B. Xu, D. Warde-Farley, et al. Generative Adversarial Nets. In Advances in Neural Information Processing Systems, volume 27. Curran Associates, Inc., 2014, URL https://papers.nips.cc/paper/2014/hash/5ca3e9b122f61f8f06494c97b1afccf3-Abstract.html.